NF

NASA TECHNICAL MEMORANDUM

NASA TM-78317

THE SWEPT ANGLE RETARDING MASS SPECTROMETER -- INITIAL RESULTS FROM THE MICHIGAN AURORAL PROBE SOUNDING ROCKET

By D. L. Reasoner, C. R. Chappell, N. H. Stone, W. E. Sharp, and J. H. Hoffman

December 1980

NASA

George C. Marshall Space Flight Center
Marshall Space Flight Center, Alabama

TECHNICAL REPORT STANDARD TITLE PAGE

1. REPORT NO.	2. GOVERNMENT ACCESSION NO.	3. RECIPIENT'S CATALOG NO.
NASA TM-78317		

4. TITLE AND SUBTITLE

The Swept Angle Retarding Ion Mass Spectrometer — Initial Results from the Michigan Auroral Probe Sounding Rocket

5. REPORT DATE December 1980

6. PERFORMING ORGANIZATION CODE

7. AUTHOR(S) D. L. Reasoner, C. R. Chappell, N. H. Stone, W. E. Sharp,* and J. H. Hoffman**

8. PERFORMING ORGANIZATION REPORT #

9. PERFORMING ORGANIZATION NAME AND ADDRESS

George C. Marshall Space Flight Center
Marshall Space Flight Center, Alabama 35812

10. WORK UNIT NO.

11. CONTRACT OR GRANT NO.

12. SPONSORING AGENCY NAME AND ADDRESS

National Aeronautics and Space Administration
Washington, D. C. 20546

13. TYPE OF REPORT & PERIOD COVERED

Technical Memorandum

14. SPONSORING AGENCY CODE

15. SUPPLEMENTARY NOTES

*University of Michigan
**University of Texas at Dallas
Prepared by Space Sciences Laboratory, Science and Engineering Directorate

16. ABSTRACT

Data from a sounding rocket flight of the Swept Angle Retarding Ion Mass Spectrometer (SARIMS) are presented to demonstrate the capability of the instrument to make measurements of thermal ions which are differential in angle, energy, and mass. The SARIMS was flown on the Michigan Auroral Probe (MAP) over regions characterized first by discrete auroral arcs and later by diffuse precipitation. The instrument measured the temperature, densities, and flow velocities of the ions NO^+ and O^+. Measured NO^+ densities ranged from 10^5 up to 3×10^5 ions/cm^3, while the measured O^+ densities were a factor of 5-10 less. Ion temperatures ranged from 0.15 up to 0.33 eV. Eastward ion flows of approximately 0.5 km/sec were measured near the arcs, and the observed flow magnitude decreased markedly inside the arcs.

17. KEY WORDS

18. DISTRIBUTION STATEMENT

Unclassified — Unlimited

David L. Reasoner

19. SECURITY CLASSIF. (of this report)	20. SECURITY CLASSIF. (of this page)	21. NO. OF PAGES	22. PRICE
Unclassified	Unclassified	19	NTIS

ACKNOWLEDGMENTS

The authors express appreciation to Dr. T. W. Shyn of the University of Michigan, Messrs. Willie Wright and Delaine Tipton of the University of Texas at Dallas, and Messrs. Larry Russell and Ronald Black of the Marshall Space Flight Center for their efforts in bringing the SARIMS from concept to reality. This work was supported in part by the National Aeronautics and Space Administration's Office of Space Science, RTOP No. 170-36-55.

TABLE OF CONTENTS

LIST OF ILLUSTRATIONS

THE SWEPT ANGLE RETARDING ION MASS SPECTROMETER— INITIAL RESULTS FROM THE MICHIGAN AURORAL PROBE SOUNDING ROCKET

I. INTRODUCTION

The report presents data on the characteristics of NO^+ and O^+ ions obtained above an active aurora measured by the Swept Angle Retarding Ion Mass Spectrometer (SARIMS). This instrument was specifically designed for low-energy ion measurements that are differential in mass, energy, and arrival angle. A protoflight instrument was flown aboard the University of Michigan Auroral Probe (MAP) sounding rocket launched on March 28, 1980, from Fort Churchill, Canada, near midnight local time.

The SARIMS represents the latest step in an evolution of low-energy ion analysis techniques which began with the OGO-V Light Ion Mass Spectrometer reported by Harris and Sharp (1969) and Chappell (1972). The original instrument consisted of a single magnetic ion mass spectrometer oriented along the spacecraft velocity vector and measured the densities of the ions H^+, He^+, and O^+ under the assumption that the plasma thermal velocity was negligible relative to the spacecraft velocity. The next step in instrument development was to add a retarding grid section for energy analysis and multiple sensor heads for flow velocity analysis. This concept was successfully demonstrated on the high-altitude SCATHA satellite (Reasoner et al., 1979). However, studies of low-energy ions from ATS-6 (Horwitz and Chappell, 1979), ISEE (Baugher et al., 1980) and SCATHA (Reasoner et al., 1979) have continued to demonstrate that magnetospheric low-energy plasma populations cannot be described in terms of simple models of convecting Maxwellian distributions; but, rather, they display complex energy and pitch angle behavior. Accordingly, the need was evident to develop an instrument with differential response in mass, in energy, and in particle arrival angle.

A sketch of the result of this development, the SARIMS, is shown in Figure 1. The SARIMS represents a merging of three separate ion analysis techniques developed for other applications. The differential angle analyzer uses a technique originally developed for analysis of laboratory plasma beams (Stone, 1977) wherein a set of deflection plates establishes an electrostatic lens to separate particles according to a range of values in energy-angle space. The HARP energy analyzer (Shyn et al., 1976) provides differential energy response with the advantage that the ratio of deflection voltage to analyzed particle energy is

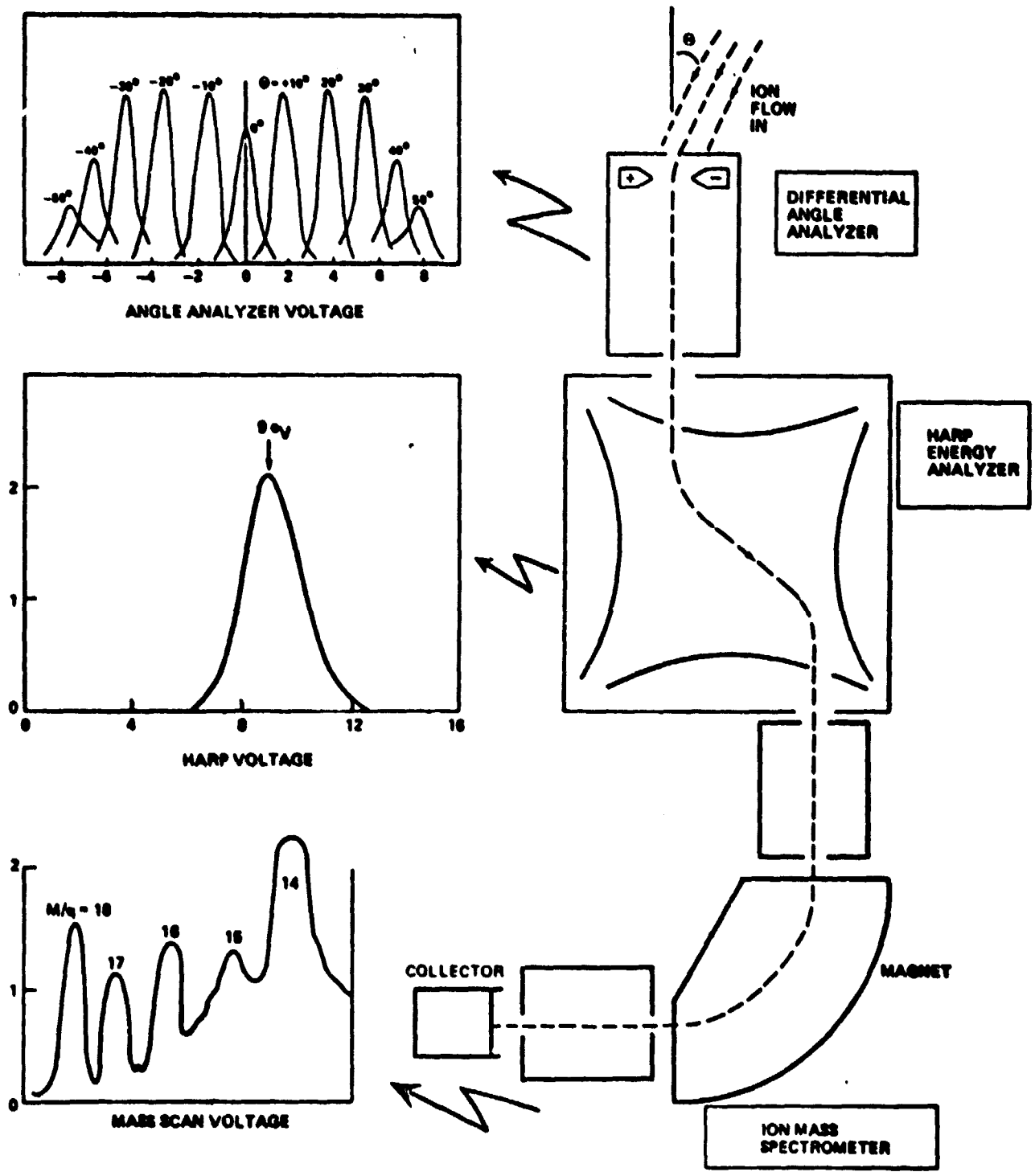

Figure 1. Diagram of the SARIMS instrument together with examples of laboratory calibration data. These data illustrate that the instrument has differential response simultaneously in the parameters angle, energy, and mass.

unity. This is important for low-energy plasma measurements because it reduces the effects of contact potential variations over the analyzer plates.

The combination of the differential angle analyzer and the HARP energy analyzer selects ions out of a distributed population with a specified range in arrival angle (10° F.W.H.M.) and with a specified range in energy ($\Delta E/E = 0.1$). Ions so selected enter the mass analyzer section and are separated in mass by a 90° sector permanent magnet mass analyzer.

The panels to the left of the figure are laboratory calibration data and are intended to illustrate the analysis capability of the SARIMS. The top panel is ion response versus angle-analyzer voltage for various values of θ, the ion arrival angle. The middle panel illustrates the energy response of the HARP, and, finally, the bottom panel is a mass analyzer scan showing prominent peaks at $m/q = 14$ (N^+) and $m/q = 18$ (H_2O^+) and illustrates the mass resolution $\Delta m/m = 0.03$.

The MAP payload was launched from Fort Churchill over an active aurora on March 28, 1980, at 0626 U.T. (0026 L.T.). Apogee was 198 km, and approximately 240 sec of flight time were above 120 km. The launch azimuth was toward the south, and the entire flight time was spent in a region of auroral precipitation. The payload was three-axis stabilized with the geometry shown in Figure 2. The y, or rocket roll axis (normally the spin axis), was aligned antiparallel to B. The x-axis was in the magnetic meridian plane pointing toward magnetic north. The SARIMS was mounted such that its F.O.V. was along the y-direction and the angle sweeping was along the z-axis. For the SARIMS data presented here, positive values of arrival angle θ corresponded to looking along the +z-axis. The payload performed three separate yaw maneuvers around the x-axis during the flight. At 0629:20 the payload yawed 100° so as to point the y-axis to the east. At 0630:00 the payload yawed 80° further to point the y-axis downward along B. The final maneuver at 0630:35 yawed the payload 180° to return the y-axis to its original orientation antiparallel to B. In essence, the payload made one complete revolution about the y-axis, stopping for 20 sec each with the x-axis looking eastward and downward.

The SARIMS was operated under control of a dedicated microprocessor. The ion species selected for analysis in this flight were O^+ ($m/q = 16$) and NO^+ ($m/q = 30$). The analysis sequence began with fixing the mass analyzer voltage for NO^+, setting the angle sweeping voltage to zero, and performing an energy scan by stepping the HARP voltage. The processor then reviewed the energy scan data and selected the energy at the peak counting rate. The HARP voltage was then fixed at that value,

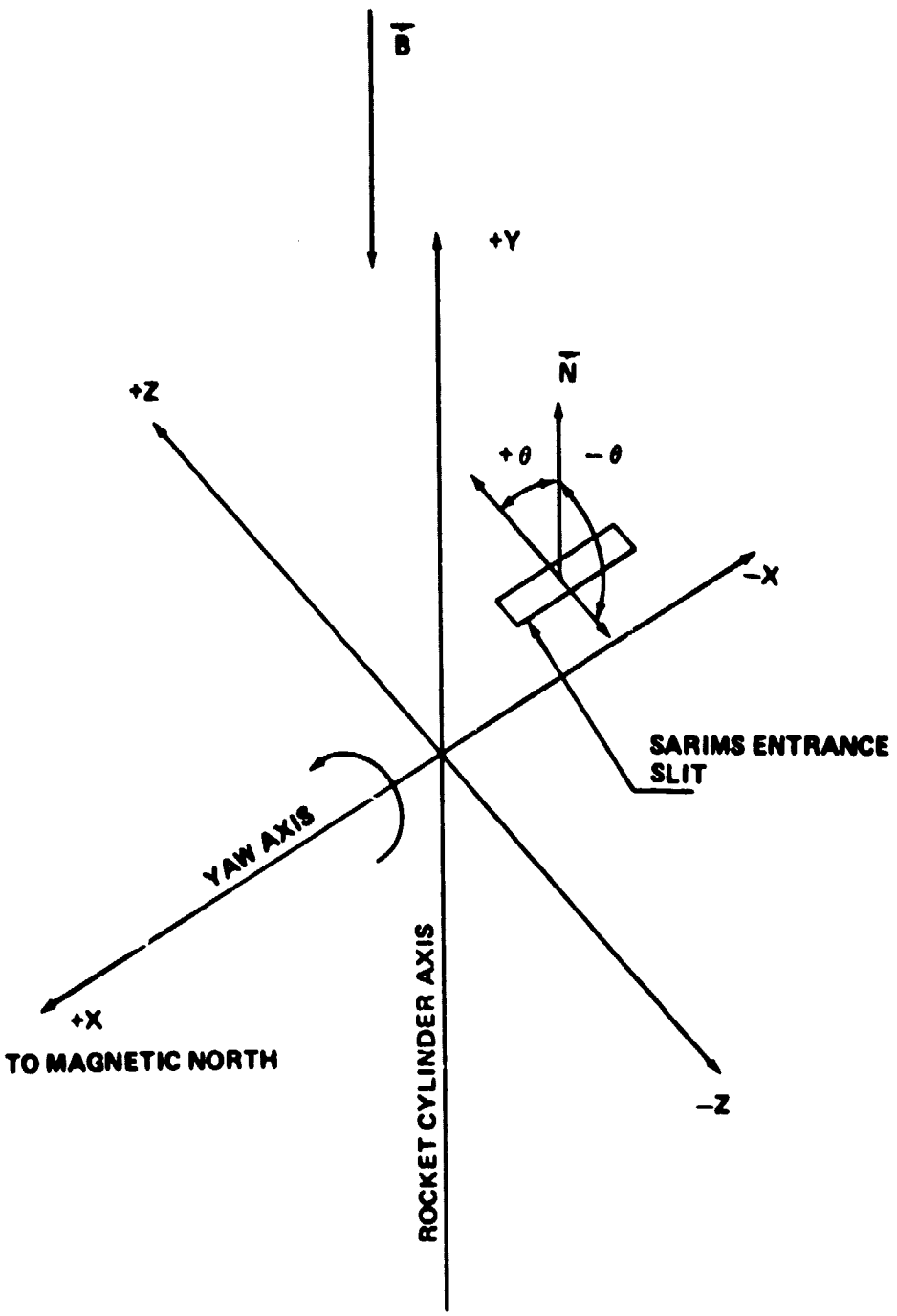

Figure 2. Geometry of the payload and SARIMS. In flight, the payload was 3-axis stabilized initially with the y-axis aligned looking upward along $\vec{B}$ and the x-axis in the magnetic meridian plane pointing toward magnetic north. The flight direction was southward. During the flight the payload performed three separate yaw maneuvers around the x-axis. These are discussed in detail in the text.

and the processor computed the differential angle analyzer voltages necessary to perform an angle scan in 5° increments from -50° to +50°. The mass analyzer was then set for O^+, and the energy scan-angle scan sequence was done for O^+. The entire cycle of analysis of the two ions was repeated every 3.3 sec.

II. DATA

Figure 3 shows an example of data from one 3-sec cycle of the SARIMS. The four panels are (top) energy and angle data for NO^+, and (bottom) energy and angle data for O^+. To facilitate comparison of peak locations and scan widths, all plots have been normalized to unity at maximum count rate. These plots illustrate several features of the data which are typical of the entire flight. The peak energy of the measured spectrum is near 1 eV, which is most probably a reflection of a negative potential acquired by the payload body in the auroral ionosphere. For this spectrum to be due entirely to the ambient ion thermal energy would require ion temperatures in excess of 10^4 °K. Such a high ion temperature is unlikely at the low altitudes of this flight where the high densities of neutral constituents would tend to keep the ion temperatures low. Also, the energy distributions shown in Figure 3 are more easily understood in terms of a cold Maxwellian accelerated to the rocket potential than a higher energy Maxwellian. The slope of the spectrum on the high energy side of the peak represents a convolution of the original ion distribution thermal width with the energy response of the instrument. The ion thermal distribution can also be estimated from the width of the angle scans, as will be discussed.

The presence of the payload potential of approximately 1 V negative with respect to the plasma and the corresponding sheath around the vehicle produced modifications to the ambient ion distribution which reached the SARIMS instrument. We saw earlier how the energy spectrum was shifted upward in energy (Fig. 3). The sheath also modified the angular distribution of the ions, and Figure 4 shows a model of this effect. The thickness of the sheath is greatly exaggerated here for clarity but, in fact, is small compared to the payload dimensions; and, hence, use of a planar geometry is justified. The sheath thickness is on the order of the plasma screening length or Debye length λ_D, and for typical ionospheric conditions at the measurement altitudes $\lambda_D \approx$ 1 cm. The ions in the unperturbed plasma are assumed to be modeled as a Maxwellian distribution with a net flow or convection velocity. Ions with velocity components in the -y direction can cross the sheath boundary and reach the rocket body. However, the approximate 1 V potential drop serves to narrow the arrival-angle range from $\pm 90°$ to smaller values $\pm\theta^{1/2}$, where $\theta^{1/2}$ is a function of the ambient ion thermal energy and of the magnitude of the potential drop. From the geometry shown, we can estimate kT_i according to:

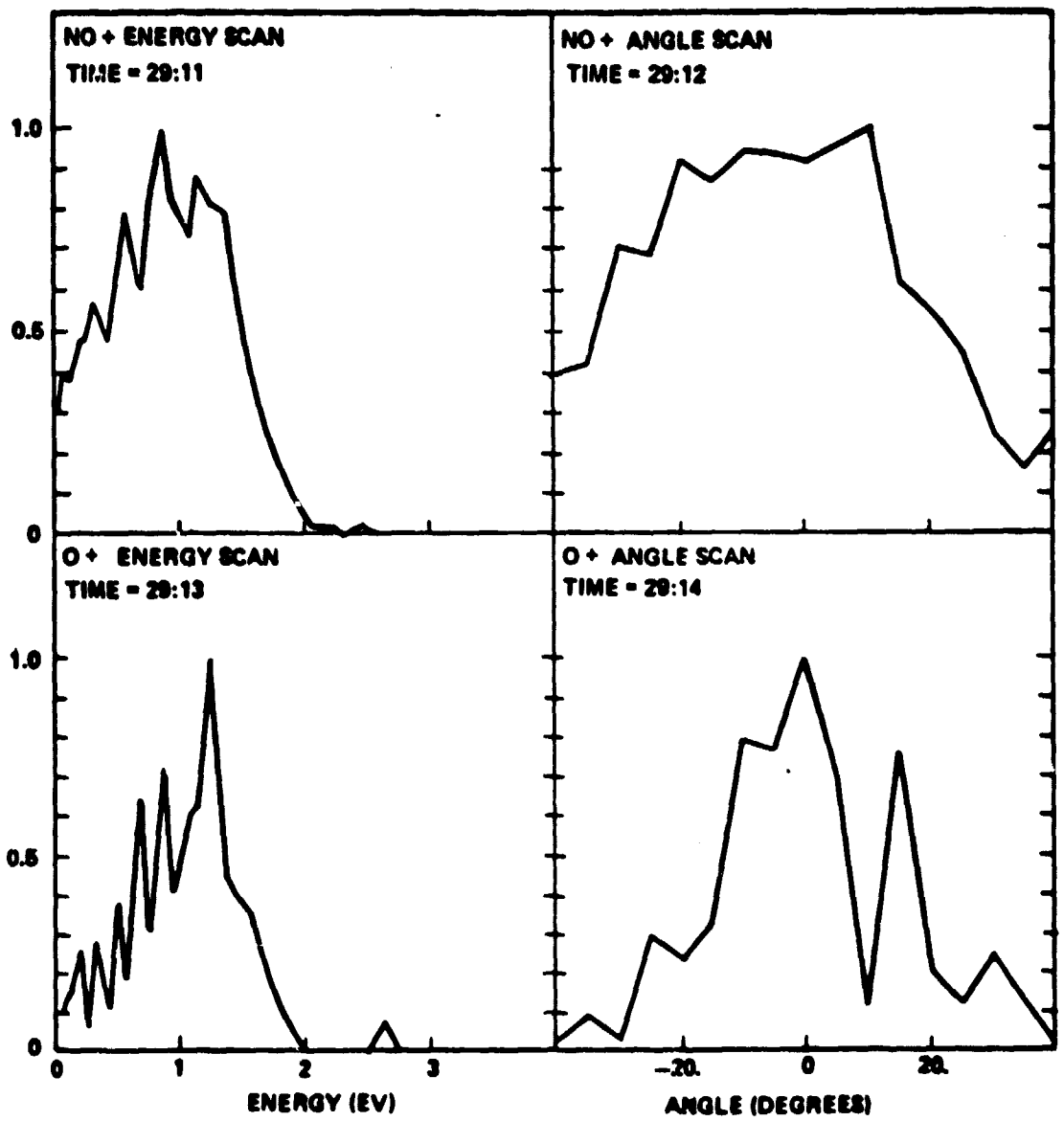

Figure 3. SARIMS data for 0629:11. At this time the payload was in a region of discrete arcs with relatively strong precipitation.

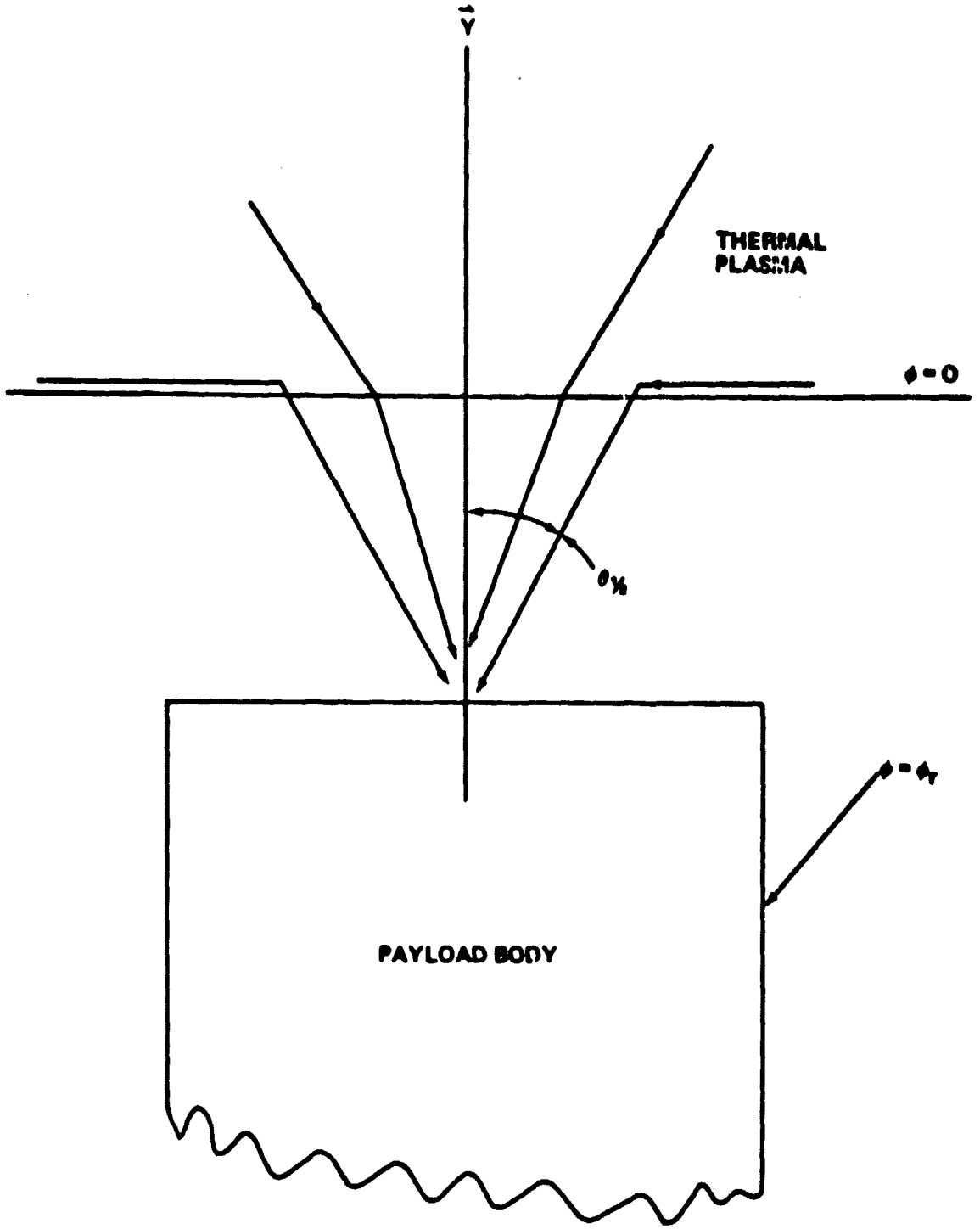

Figure 4. Model of the sheath surrounding the payload used for estimating the ambient ion temperature. The action of the payload attractive potential ϕ_T is to transform the ions initially from an arrival-angle range of ±90° to a range ±θ which is a function of ϕ_T and the ambient ion temperature.

$$\theta^{1/2} = \tan^{-1}\left(\frac{kT_i}{q\phi_r}\right)^{1/2}$$

where $\theta_{1/2}$ is the half-width of the angle scan and ϕ_r is the rocket body potential. In the example shown in Figure 3 for NO^+, $\theta_{1/2} = 29°$, implying $kT_i = 0.33$ eV. For O^+, $\theta_{1/2} = 18°$, implying $kT_i = 0.12$ eV.

Another point of interest in the data shown in Figure 3 is that the energy spectra for O^+ ions are well modeled by a thermal distribution shifted by a 1 V potential and then convolved with the HARP energy response. The NO^+ spectra, however, generally show a skew toward lower energies, and this implies that some fraction of the NO^+ ions did not experience the full potential drop between the unperturbed plasma and the payload body.

One possible interpretation of these data is that a significant fraction of the observed NO^+ ions were created in the sheath surrounding the rocket. Examination of the NO^+ spectra shows that typically approximately 20 percent of the NO^+ ions did not receive the full potential drop. This would mean that the NO^+ production rate would have had to have been such that 20 percent of the ambient density would have been formed in the time required for the rocket to traverse a distance equal to the sheath dimension. Assuming a sheath dimension of 10 cm and rocket velocity of 5×10^4 cm/sec, this would imply an NO^+ production rate of approximately 5×10^8 ions/cm^3-sec. This production rate seems excessively high, as typical loss rates through dissociative recombination for NO^+ are in the range of $10^4 - 10^5$ ions/cm^3-sec. An alternate interpretation may be that the NO^+ spectra are being modified by local processes in the sheath. This question remains unresolved.

We note that late in the flight the NO^+ spectra changed character, specifically after 30:30 when the rocket had passed out of the region of discrete arcs with intense precipitation to a region of diffuse lower intensity precipitation. Figure 5 shows an example of data at 31:21 and is the same format as Figure 3. Here, we see that both the NO^+ and O^+ spectra are consistent with shifted Maxwellian distributions and that the angle scans for both ions were essentially the same in terms of width and lack of significant offset. As was done earlier for the data in Figure 3, here the ion thermal energy was calculated from the width of the angular scan, and the result was $kT_i(NO^+) \approx kT_i(O^+) = 0.15$ eV or an equivalent temperature of 1740 °K.

The magnitude and direction of the convection or flow velocity component along the payload z-axis (see Fig. 2) can also be computed by

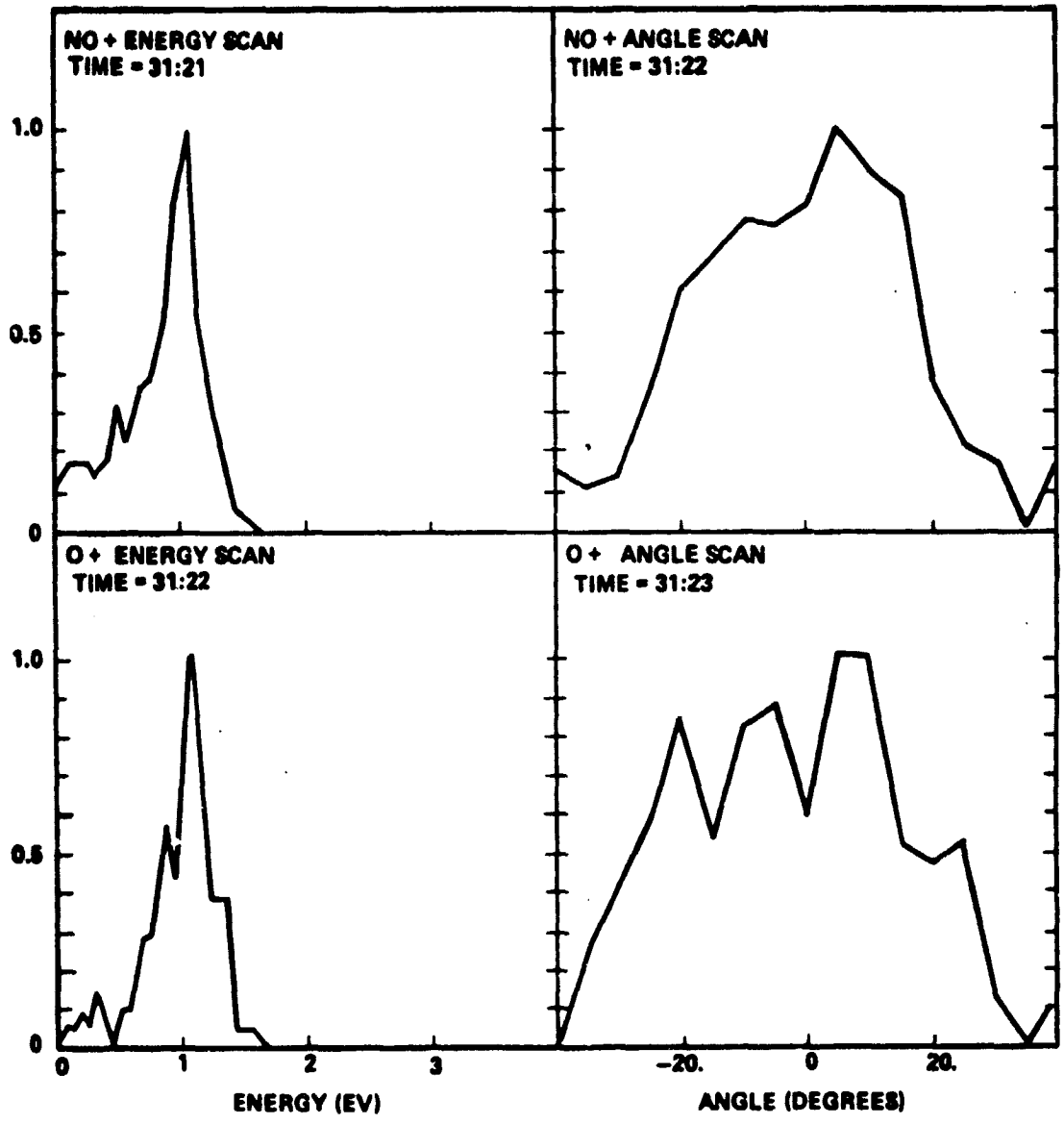

Figure 5. Flight data at 0631:21. Late in the flight the payload was in a region of diffuse precipitation.

measuring the offset θ' of the angle-scan from 0°. The flow velocity V_F can be computed from the offset angle θ' according to:

$$V_F = \left(\frac{2q\phi_r}{m_i}\right)^{\frac{1}{2}} \tan \theta' \quad .$$

For the purpose of data analysis, Gaussian distributions were fit to the NO^+ and O^+ angle scans to obtain the best estimates of the parameters $\theta_{\frac{1}{2}}$ (angle scan width) and θ' (offset angle). The instrumental angle width of 10° F.W.H.M. was always considerably less than the values of $\theta_{\frac{1}{2}}$ and represented only a small correction to the fitted values of $\theta_{\frac{1}{2}}$, in any case within the error limits of the fit, which was $\pm 2°$.

Summary plots were made for the entire flight with the parameters NO^+ peak count rate, O^+ peak count rate, peak energy of NO^+, and the offset angles for both NO^+ and O^+. There are gaps in the O^+ data at the beginning and ending of the flight because of low count rates and, hence, poor statistics. The peak energy for O^+ essentially tracks that of NO^+ and is not shown. Data for the electron energy flux integrated over electrons with energies from 10 eV to 10 keV were also obtained (J. D. Winningham, private communication). These plots are shown in Figure 6. Also shown are the times for the payload yaw maneuvers discussed earlier. This energy flux plot shows that for essentially the entire duration of the rocket flight the flux was 1 erg/cm^2-sec or greater.

Although difficult to discern here because of the plotting scale, examination of detailed electron spectral information from the electron spectrometer on the payload (Winningham, private communication) showed structured arcs centered at 29:10, 29:40, and 30:10. These intervals are indicated on the plot.

After 30:30, the payload entered a region of diffuse precipitation with a strong pitch-angle modulation indicating a precipitating distribution with a characteristic energy of 3-4 keV. Recalling that the payload was traveling southward, we interpret the data to indicate that initially the payload was in a region of highly structured arcs and about 30:30 passed into the diffuse plasma sheet precipitation region.

It is seen that the general trend is for the NO^+ and O^+ fluxes and the payload potential, as shown by the increasing peak energy of NO^+, to follow the electron energy flux. The sustained peak energy increase that occurred between 30:35 and 31:10 was during a 180° yaw motion of the rocket when the projected payload area perpendicular to the magnetic field went through a maximum as the rocket axis was at 90° to

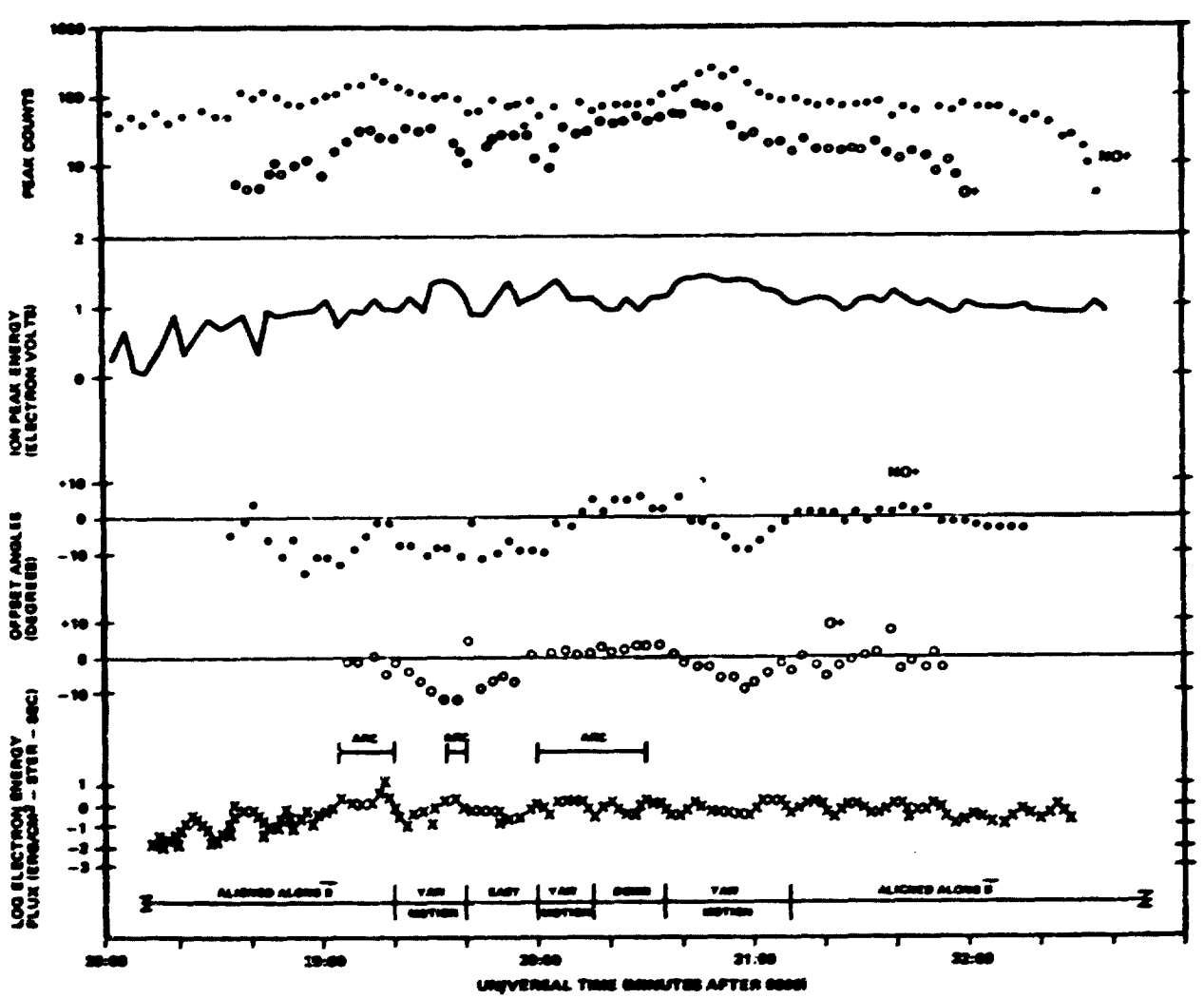

Figure 6. Summary plots of the flight data. The top two traces are the peak counts for NO^+ and O^+ ions and illustrate the general data trends. The next panel is the peak energy of the NO^+ ions and is essentially a measure of the payload potential. The next two traces are the offset angles and are a measure of flows of NO^+ and O^+. The electron energy flux for electrons between 10 eV and 10 keV is shown in the bottom panel.

the field. The electron measurements indicated a strongly field-aligned precipitating distribution; and, as the high energy electron flux to the rocket reached a maximum, this forced the payload potential to a larger negative value, resulting in an increase in the NO^+ peak energy.

We turn now to a discussion of the ion flows as measured by the offset angles of the angle scans. The error limits of the fitted values of offset angles are $\pm 2°$. It is apparent from examining Figure 6 that periods of sustained ion flows along the payload z-axis were observed. From a first-order perspective we can clearly see the changes in flow direction as the payload yawed first in two separate 90° maneuvers at 29:20 - 29:40 and 30:30 - 30:15 and, finally, in a single 180° maneuver from 30:35 - 31:10. At 29:00 the payload was north of an arc, and a significant flow from west to east was observed. The computed flow velocity is 0.53 ± 0.1 km/sec, corresponding to an electric field of 26 mV/meter. This flow direction and magnitude are in general agreement with flows measured by the Chatanika Radar Facility near midnight around auroral arcs (Horwitz et al., 1978). As the arc was traversed, the convection velocity was seen to decrease. Immediately after exiting the arc, the payload began the first of the three yaw maneuvers, stabilizing at 29:40 with the payload y-axis pointing east.

The SARIMS, therefore, was scanning up and down along the magnetic field line. Here, the angle offset indicated a net flow of ions downward relative to the payload with a velocity of 0.44 ± 0.1 km/sec. At this time, the vertical velocity was 0.36 km/sec upward; hence, the measured relative ion velocity is consistent with having been entirely due to the payload motion. The payload again began a yaw maneuver at 30:00 to point the y-axis downward, and we see that the measured angle offset is small and slightly positive. Here, the payload was inside an auroral arc region. Since the payload and, therefore, the SARIMS scan directions had reversed relative to geographic coordinates, this indicated an eastward flow but at a smaller magnitude than the flow observed around 29:00. The calculated flow velocity was 0.22 ± 0.09 km/sec. At 30:30, the payload entered a region of diffuse precipitation. The final yaw maneuver, which began at 30:35, was marked by excursions in the offset angles of both O^+ and NO^+ ions which reached a maximum when the payload y-axis was at 90° relative to the magnetic field line. The negative excursion indicated a flow upward relative to the payload of 0.47 ± 0.11 km/sec, and this is consistent with the rocket vertical velocity of 0.36 km/sec downward at this time.

In summary, the flow data showed eastward flows of approximately 0.5 km/sec northward of a region of discrete arcs, but the flow magnitude decreased markedly inside the arcs. To the south of the region of discrete arcs, in a region of diffuse precipitation, no flow could be discerned. As the payload yawed so that the SARIMS was scanning up and

down along field lines, flow components were seen. These were consistent with having been entirely due to the payload vertical motion. The SARIMS instrument was effective in measuring this relative ion motion and can be expected to function successfully anywhere in auroral conditions where the flows are greater than approximately 0.1 km/sec. This minimum flow sensitivity was set by the angle error limits of $\pm 2°$ and by the effects of the payload sheath and negative potential which imparted a significant velocity (2.5 km/sec) to the ions. In future flights the instrument entrance aperture will be biased near plasma potential, and in this case the velocity perturbation will be the payload ram velocity of approximately 0.5 km/sec. This can reduce the minimum observable flow velocity to as low as 20 m/sec.

The final aspect of the data analysis concerns computation of the absolute density of the NO^+ and O^+ ions. The payload is at a potential relative to the plasma which is several times the thermal energy of the ions, and this produces considerable modifications to the equations for calculation of density. The problem is made manageable by the fact that the SARIMS instrument has a narrow-angle field-of-view, $10° \times 15°$, equivalent to a conical field-of-view with a half-angle of $\alpha = 6.9°$. Under these conditions of small angle it can be shown (Singh and Baugher, 1980) that:

$$\frac{J}{J_o} = \left(1 + \left|\frac{q\Phi_r}{kT}\right|\right) \sin^2 \alpha$$

where J is the flux reaching the instrument, $J_o = N\,(kT/2\pi m)^{\frac{1}{2}}$ is the hemispherical flux crossing the plasma sheath boundary, and α is the instrument field-of-view half-angle.

Using this formulation, we compute the following values for the NO^+ and O^+ densities from the data shown in Figures 3 and 6. At 29:11 (Figure 3) the results were $N(NO^+) = 2.8 \times 10^5$ and $N(O^+) = 2.9 \times 10^4$ ions/cm^3. Later in the flight at 31:21 (Fig. 6), the results were $N(NO^+) = 1.0 \times 10^5$ and $N(O^+) = 1.5 \times 10^4$ ions/cm^3. These values are entirely reasonable in light of present models of the auroral ionosphere.

III. SUMMARY AND CONCLUSIONS

The data from this initial SARIMS flight have demonstrated the basic capability of the instrument to make measurements of thermal and suprathermal ions which are differential in angle, energy, and mass. These capabilities become especially important in the typical situations

in spacecraft thermal ion measurements where the spacecraft potential is not at plasma potential. The differential mass capability allows a single ion specie to be selected. The differential energy capability allows measurement of the ion energy distribution and the spacecraft potential in the case of attractive potentials. Perhaps most importantly, the differential angle capability allows measurements of the ambient distribution properties and of the modifications of ion trajectories in the sheath region. It is important also to notice that the angle scanning is done electrically so that the entrance aperture remains at a fixed location relative to the spacecraft. This is particularly important in the case where sheath dimensions are small compared to the spacecraft dimensions.

Prior to this flight the different components of the SARIMS instrument had been subjected to extensive testing, both on rockets and in the laboratory. This testing, however, had been carried out on separate elements of the analyzer section. This flight gives a successful verification of the combined SARIMS concept in space under disturbed auroral conditions and adds further confidence in the use of this technique on rocket and satellite missions. In fact, the auroral ionosphere is in a sense a worst case in comparison to the rest of the magnetosphere, since the ion temperatures are typically less than 0.5 eV. The HARP energy analyzer will easily be able to measure the higher temperature suprathermal plasma components found in the magnetosphere.

The measured values of ion densities, temperatures, and flow velocities are all very reasonable and give a high level of confidence in the basic operating principles of the instrument. The utility of adaptive scanning, wherein the angle scans were done after locating the peak energy, was clearly demonstrated. Techniques such as this become extremely important as instruments become more complex and the need to make the most efficient use of the available telemetry becomes paramount.

Future applications of the SARIMS to measurements of thermal and suprathermal ions in other magnetospheric regions such as on the OPEN mission will require some refinement in order to increase the geometric factor to compensate for lower plasma densities. Such an effort would be well repaid by the wealth of new information that would be received on the detailed characteristics of the low-energy ion populations in the magnetosphere.

REFERENCES

Baugher, C. R., Chappell, C. R., Horwitz, J. L., Shelley, E. G., and Young, D. T.: Initial Thermal Plasma Observations from ISEE-1. To be published in Geophys. Res. Letters, September 1980.

Chappell, C. R.: Recent Satellite Measurements of the Morphology and Dynamics of the Plasmasphere. Rev. Geophys. Space Phys., 10, 951, 1972.

Harris, Kent K. and Sharp, Gerald W.: OGO-V Ion Spectrometer. IEEE Trans. Geosci. Elect., GE-7, 93, 1969.

Horwitz, J. L., Doupnik, J. R., and Banks, P. M.: Chatanika Radar Observations of the Latitudinal Distributions of Auroral Zone Electric Fields, Conductivities, and Currents. J. Geophys. Res., 1463, 1978.

Horwitz, J. L. and Chappell, C. R.: Observations of Warm Plasma in the Dayside Plasma Trough at Geosynchronous Orbit. J. Geophys. Res. 84, 7075, 1979.

Reasoner, David L., Craven, Paul D., and Chappell, C. R.: Observations of Spacecraft-Plasma Interactions Near Synchronous Orbit. EOS, Trans. Am. Geophys. Union, 60, 923, 1979.

Shyn, T. W., Sharp, W. E., and Hays, P. B.: Gridless Retarding Potential Analyzer for Use in Very Low Energy Charged Particle Detection. Rev. Sci. Instrum., 47, 1005, 1976.

Singh, Nagendra and Baugher, Charles R.: Sheath Effects on Current Collection by Particle Detectors with Narrow Acceptance Angles. To be published in Space Sci. Instrum., 1980.

Stone, Nobie H.: Technique for Measuring the Differential Ion Flux Vector. Rev. Sci. Instrum., 48, 1458, 1977.

APPROVAL

THE SWEPT ANGLE RETARDING ION MASS SPECTROMETER-- INITIAL RESULTS FROM THE MICHIGAN AURORAL PROBE SOUNDING ROCKET

By D. L. Reasoner, C. R. Chappell, N. H. Stone, W. E. Sharp, and J. H. Hoffman

The information in this report has been reviewed for technical content. Review of any information concerning Department of Defense or nuclear energy activities or programs has been made by the MSFC Security Classification Officer. This report, in its entirety, has been determined to be unclassified.

Charles A. Lundquist

CHARLES A. LUNDQUIST
Director, Space Sciences Laboratory

☆ U.S. GOVERNMENT PRINTING OFFICE 1980—740-066/262 REGION NO. 4